59th ILMENAU SCIENTIFIC COLLOQUIUM
Technische Universität Ilmenau, 11 – 15 September 2017
URN: urn:nbn:de:gbv:ilm1-2017iwk-025:1

Requirements and Potentials of Human Kinetic Energy Harvesting Technologies with Focus on Electromagnetic Conversion Methods

Oliver Kröning and Hendrik Rothe

Chair of Measurement and Information Technology
Helmut Schmidt University / University of the Federal Armed Forces
Hamburg, Germany

ABSTRACT

In the recent years, energy harvesting has become increasingly popular for powering low-energy devices. Therefore, human power has become a promising energy source in providing electrical energy. Thus, the general principles, structures, requirements and potentials of human kinetic energy harvesting technologies are presented.
Commonly, human kinetic energy harvesting systems have to be adjusted to the human locomotion. For the purpose of maximizing the power output, results of biomechanical analyzing methods are presented to identify resonant frequencies and bandwidths.
With focus on inertial electromagnetic generators, further challenges and potentials are discussed to optimize the power conversion. In doing so, mechanical and electrical characteristics of the generator structure are examined and optimization problems are derived. One major issue within power maximizing is to match the resonant frequency and achieve a suitable electromechanical coupling. Parameter dependencies are identified by using analytic and numerical representations of generic electromagnetic generators.

Index Terms – human kinetic energy harvesting, electromechanical conversion, electromagnetic, human motion, design criteria

1. INTRODUCTION

The demand for electrical energy, especially in mobile and off-grid applications, has increased within the recent years. The development of portable devices and stand-alone systems as smartphones, automobiles, unmanned aerial vehicles and wireless sensor networks requires powerful, efficient and self-contained sources of energy. Additionally, micro-applications are limited in size and weight; hence, a compact, lightweight and low-cost energy provision is needed. [1] [2]
Generally, these electronics are supplied by batteries and accumulators. However, there are several drawbacks concerning the practical use of electrochemical energy sources. Due to limited battery capacities, an intermittent replacement and maintenance have to be ensured for long-term operation corresponding systems. Especially in aerospace and meteorological applications, the self-sufficient supply of maintenance-free energy has become a major issue. Furthermore, the disposal of electrochemical elements has environmental impacts. [3] [4] [5]
In recent years, energy harvesting has become an interesting field of research opening alternative ways of energy provision and hence new options for mobile and/or wireless applications. The conversion of unconventional forms of ambient energy, like solar, thermal or radio frequency energy into electricity enables a cost-efficient implementation of power supplies within energy-autonomous devices. [6]

Therefore, biomechanical or human kinetic energy harvesting systems utilize the kinetic energy provided by human body motions and locomotion. The human body is a vast reservoir of energy and provides a lot of potentials to perform mechanical or thermal work. This power can be harvested by using suitable devices to primarily supply portable electronics or implantable body sensor with electricity. [7] [8]
In general, the optimal design of electromechanical energy harvesting systems depends on the source of energy and its characteristics. Forces and accelerations affecting biomechanical energy harvesters during walking and running have to be evaluated to adjust the systems' parameters in order to maximize the power output. Mitcheson et al. [9] presented three types of vibration-based micro generator architectures with the assumption of sinusoidal excitation. However, human movement provides a broad spectrum of sinusoidal components, which are difficult to harvest simultaneously [10]. Thus, the mechanical subsystem of the energy harvesting system needs to be adapted to the frequency response of the moving body. Furthermore, the conversion of mechanical energy into electrical energy requires a suitable harvesting method, which is dependent on several parameters as well.
The aim of this paper is to clarify potentials and requirements of human kinetic energy harvesting methods. Considerations about the energy source and design parameters of harvesting devices support the prospective development and dimensioning of biomechanical generators. This includes a presentation of gait analyses in section 2 to derive design features of the electromechanical conversion. Afterwards, section 3 gives information about the basic structure of vibration-based energy harvesting systems as well as the power considerations within these devices. Presented models of generic electromechanical systems express the dependence of the output power on parameters of the systems and the source. Since our future work focusses on the development of electromagnetic inertial generators, sections 4 and 5 present a basic electromagnetic power conversion model as well as a parameter study to find further design criteria in order to identify optimization methods. The derivation of requirements and challenges in designing electromagnetic energy harvesting systems based on preceding sections is then presented in section 6, followed by a conclusion in section 7.

2. BIOMECHANICAL ANALYSES

In the field of human kinetic energy harvesting, biomechanical analyses are essential to find potentials of scavenging power. Therefore, optimal body positions for the attachment of harvester devices have to be identified. Regarding electromechanical power conversion, body positions where high accelerations and forces as well as large displacements occur during walking and/or running are required to obtain a high power output. In von Büren et al. [11] different architectures of inertial micropower generators were tested at nine body locations. As a result, generators attached at lower body locations provided a power output four times higher than harvester devices mounted at the upper body during walking. Thus, our biomechanical analysis focus on lower body positions as ankle, knee and hip.

2.1 Biomechanical Analyzing System

A method for biomechanical analyses using IMUs (inertial measurement units) as well as their fusion with optical sensors is presented in Kröning et al. [12]. The associated experimental setup is depicted in Figure 1. With the usage of a high-speed camera, positional data of markers at hip, knee and ankle are measured. Thereby, two-dimensional marker displacements within the recorded images are obtained and projected onto the global frame. Thus, it is assumed that every movement is limited to the sagittal plane. Displacements perpendicular to the sagittal plane are neglected.

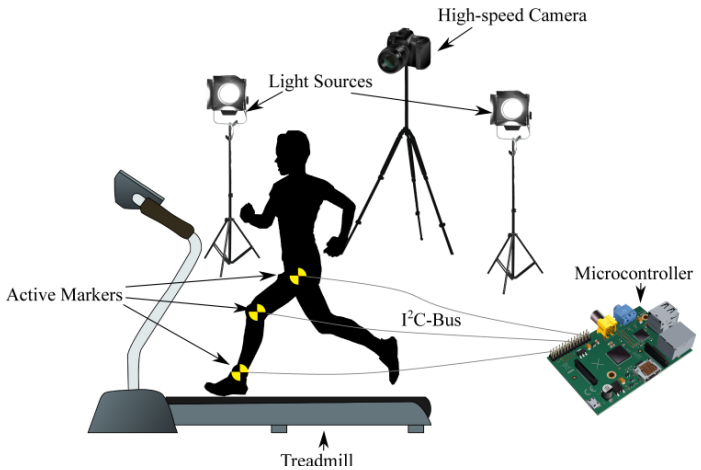

Figure 1: Experimental setup for human gait analysis using IMUs and their fusion with optical sensors.

To measure acceleration and angular velocity at the mentioned body positions, microcontroller operated IMUs within the markers are applied. The obtained IMU data are used to estimate the orientation of the sensor. Additionally, magnetometer information is fused with the accelerometer and gyroscope data using an efficient filter approach [13] to obtain a complete measurement of orientation with respect to gravity. Due to the torque at the joints, the markers' orientations change during the gait cycle. Orientation estimation supports the identification of suitable body locations, because linear accelerations (accelerations based on dynamic motions without the impact of gravity) can be calculated within the sensor frame. To synchronize and fuse the measured linear acceleration and recorded high-speed camera images, LED-based active markers are used.

2.2 Results of human gait analysis

It should be mentioned that different body sizes and proportion generate different results within the human gait analysis due to, e.g., longer or shorter leg sizes of the test person (subject). Our gait analysis was performed on a 35 year old subject with a size of 1.70 m and weighting 65 kg. In each series of measurement, the subject walks or runs three times at a predefined velocity of v_{gait}=5…12 km/h for a measurement time of T_{meas}=4 s.

First, the markers' displacements in the global frame (distinguished by a superscripted *E*) as a result of the optical tracking method are considered. Therefore, the zero-mean positional data for ankle, knee and hip at two different velocities are shown for comparison in Figure 2. It is obvious that walking motion produces lower vertical displacements (^{E}y) than running. Further, the ankle generates by far the highest displacement amplitude during the gait cycle compared to knee and hip motions. However, the vertical knee and hip displacements significantly increase during running due to jump movements within the gait cycle.

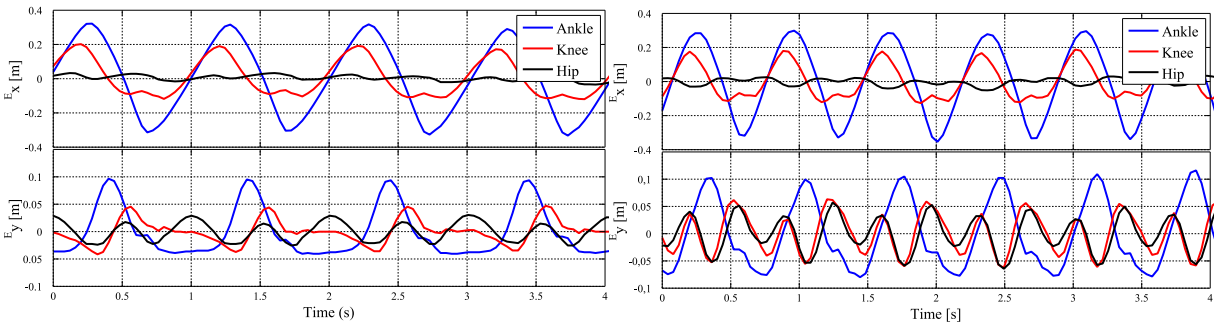

Figure 2: Zero-mean displacements of markers during walking (left) at v_{gait}=5 km/h and running (right) at v_{gait}=10 km/h.

The absolute linear acceleration over all three dimensions within the sensor frame (^{S}x, ^{S}y, ^{S}z) of the markers is depicted in Figure 3. The ankle movement produces the highest peaks at the initial contact – the short time period when the heel touches the ground. This acceleration increases during running, because the entire weight of the body rests only on the heel when the subject performs a jump movement. The accelerations at hip and knee are comparatively low during walking. However, the knee's absolute acceleration while running is almost similar to acceleration of the ankle in Figure 3 (right). A detailed perspective is obtained by regarding the horizontal and vertical component of the linear acceleration of ankle and knee in Figure 4. Most of the ankle acceleration is performed in the vertical component in sensor frame due to the initial contact of the foot. By contrast, the knee acceleration splits in two components during running motion, because of jumping forward within the gait cycle.

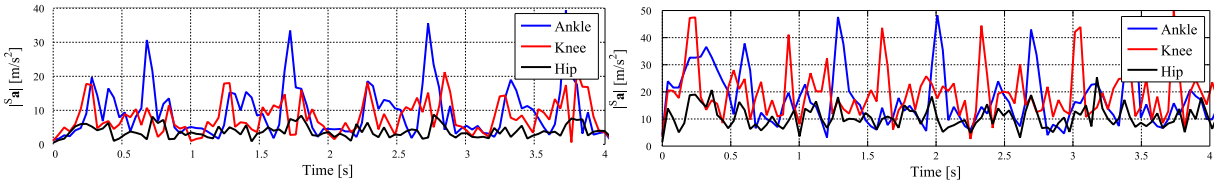

Figure 3: Absolute linear acceleration of markers in sensor frame at ankle, knee and hip during walking (left) at v_{gait}=5 km/h and running (right) at v_{gait}=10 km/h.

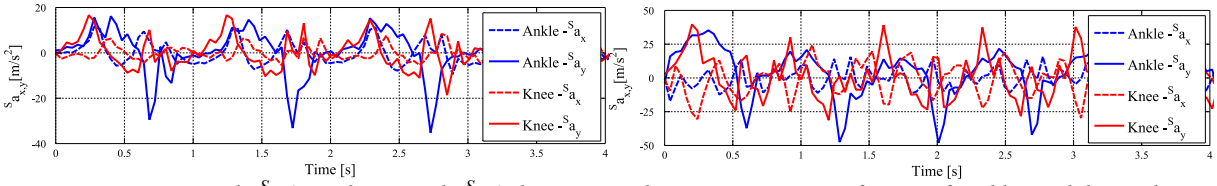

Figure 4: Horizontal ($^{S}a_x$) and vertical ($^{S}a_y$) linear acceleration in sensor frame of ankle and knee during walking (left) at v_{gait}=5 km/h and running (right) at v_{gait}=10 km/h.

The frequency characteristics of the acceleration at potential body positions are essential for specifying internal harvester parameters. Therefore, Figure 5 (left) shows the frequency response for ankle and knee during walking (v_{gait} = 6 km/h) and running (v_{gait} = 10 km/h). The ankle's principal maximum is located at 1 Hz for walking, which is approximately the cadence of the subject's walk. The maximum of the knee's acceleration is located at 2 Hz and hence higher. It is apparent that a frequency shift occurs in the frequency response of the running motion. This shift is approximately 0.4 Hz for the ankle's maximum and 0.8 Hz for the knee's maximum. The frequency shift is depicted in detail in Figure 5 (right). Here, the ankle's frequency response is shown at different gait velocities, whereby $\Delta f_1 \approx 0.6$ Hz and $\Delta f_2 \approx 1.2$ Hz are measured for the frequency shifts of the first and second maximum.

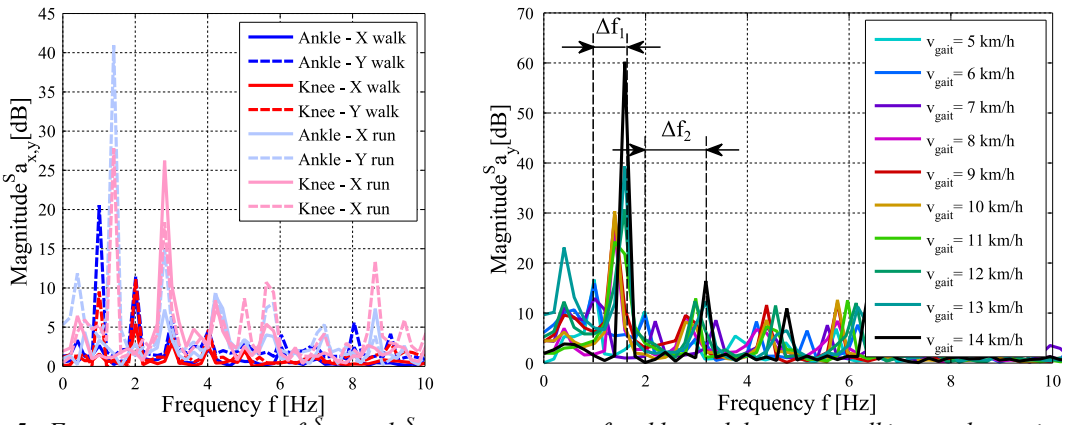

Figure 5: Frequency response of $^{S}a_x$ and $^{S}a_y$ components of ankle and knee at walking and running (left). Frequency shift of ankle's $^{S}a_y$ component during gait cycle at different velocities (v_{gait}=5…14 km/h) (right).

3. BASICS OF ELECTROMECHANICAL CONVERSION

3.1 General Structures

Kinetic or vibration energy harvesting systems utilize the relative movement between objects to convert mechanical energy into electrical energy. The conversation is realized by implementing a damping or harvesting technology. Relative movements are generated in motors and turbines in an industrial environment or, in our case, during the human gait. To harvest mechanical power $p_{mech}(t)$ via a force acting with a certain velocity of the relative motion

$$p_{mech}(t) = F_a(t) \cdot \dot{z}(t) \,, \tag{1}$$

a harvesting structure as depicted in Figure 6 has to receive the mechanical energy. Therefore, direct-force and inertial mass generators are usually applied for energy conversion. Both are structured as 1-DOF spring–mass–damper systems with proof mass m, damping coefficient c and spring stiffness k. The generic structures differ in the cause of the displacement of the proof mass $z(t)$ relative to the housing. Within direct-force energy harvesting systems, the suspended mass is directly affected by the driving force $F_a(t)$. In contrast, the operating principle of inertial mass generators is based on the inertia of the suspended mass when the housing is accelerated by an external force. In both cases, a force opposing the mass' motion is provided by the implemented damper c which enables the conversation into electric power. Inertial mass generators seem to be more flexible compared to direct-force generators as only one point of attachment to the moving body is required. [14] Thus, more types of inertial based systems are documented than direct-force approaches. Our future work also focusses on inertial mass generators. Hence, further considerations only deal with this kind of system.

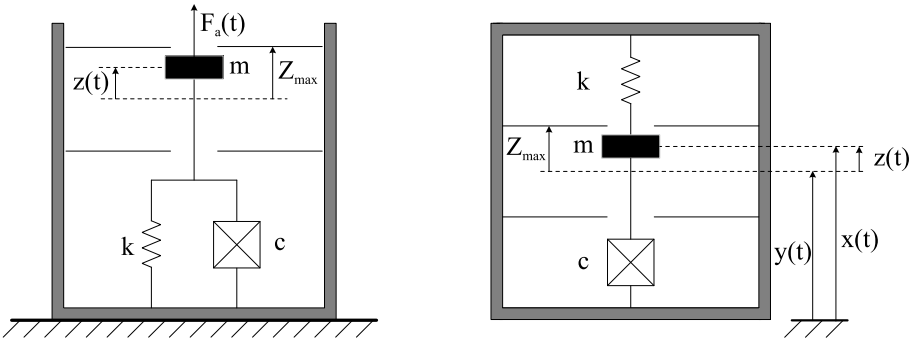

Figure 6: Structures of generic kinetic energy harvesting approaches according to Mitcheson et al. [14]. Direct-force generator (left); inertial mass generator (right).

3.2 Power Considerations

A suitable model of inertial mass energy harvesting systems can be found in Williams et al. [15] and El-hami et al. [16]. According to Newton's second law of motion, the governing differential equation is given by [17]

$$m\ddot{z}(t) + c\dot{z}(t) + kz(t) = -m\ddot{y}(t) \,, \tag{2}$$

whereby $y(t)$ is the excitation of the housing. Neglecting the mass of the device's frame, the excitation force is $F_a(t) = -m\ddot{y}(t)$. Assuming a harmonic excitation $y(t) = Y \sin(\omega t)$ with amplitude Y and angular frequency $\omega = 2\pi f$, equation (2) becomes

$$m\ddot{z}(t) + c\dot{z}(t) + kz(t) = m\omega^2 Y \sin(\omega t) \,. \tag{3}$$

According to Stephen [18], a steady-state solution of the proof mass' relative displacement is given by $z(t) = Z \sin(\omega t - \varphi)$ with the vibrational amplitude

$$Z = \frac{m\omega^2 Y}{\sqrt{(k-\omega^2 m)^2+c^2\omega^2}} \tag{4}$$

and phase angle

$$\varphi = \tan^{-1}\left(\frac{c\omega}{k-m\omega^2}\right). \tag{5}$$

Since the instantaneous power transfer is given by equation (1), the average extracted power P_d within the damper, which consists of mechanical and electrical components, can be calculated by using the opposite damping force given by c and the velocity of the relative motion $\dot{z}(t)$. Substituting the amplitude from equation (4) leads to [18]

$$P_d = \frac{1}{2}c\omega^2 Z^2 = \zeta m\omega_n\omega^2 Z^2 = \frac{cm^2\omega^6 Y^2}{2((k-\omega^2 m)^2+c^2\omega^2)}. \tag{6}$$

Another form of equation (6) can be expressed by

$$P_d = \frac{m\zeta Y^2\omega_c^3\omega^3}{(1-\omega_c^2)^2+(2\zeta\omega_c)^2}, \tag{7}$$

where $\omega_c = \omega/\omega_n$ represents the ratio of excitation frequency ω of the vibration source and the resonant frequency of the spring–mass–damper system

$$\omega_n = \sqrt{\frac{k}{m}}. \tag{8}$$

In practice, the system's damping coefficient c changes with mass and resonant frequency and cannot be assumed as constant. To take this into account within the power consideration, the damping ratio ζ is introduced in equations (6) and (7). It is defined as

$$\zeta = \frac{c}{2m\omega_n} = \zeta_e + \zeta_{par}. \tag{9}$$

The damping ratio ζ regards electrical damping ζ_e, which occurs during the conversion into electricity, and parasitic damping ζ_{par}, e.g. due to mechanical (air resistance) or electrical (parasitic impedances) effects.

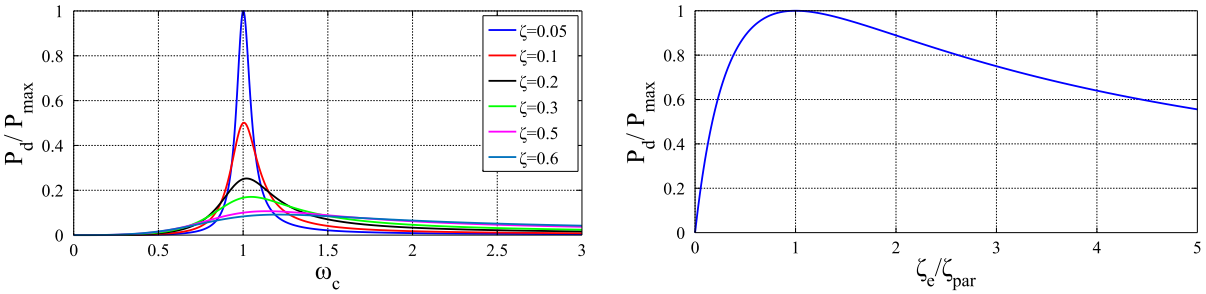

Figure 7: Normalized power depending on the frequency ratio ω_c (left) and ratio of ζ_e/ζ_{par} (right).

In Figure 7, the normalized power from equation (7) is shown. Obviously, the maximum power is received at resonance condition $\omega_c = 1$. Thus, a matching of the system's resonant frequency to the excitation frequency of the vibration source ($\omega_n = \omega$) is required.
Additionally, Figure 7 illustrates the complex influence of the total damping ratio ζ. First, low damping ratios cause high power output at resonance condition. However, the bandwidth[1] $\Delta\omega = 2\pi(f_{c,2} - f_{c,1})$ of output power P_d decreases with lower damping ratios. Therefore, the quality factor connects the system's bandwidth with its damping ratio:

$$Q = \frac{1}{2\zeta} = \frac{\omega_n}{\Delta\omega}. \tag{10}$$

With equations (8) and (9), we obtain the expression

[1] The bandwidth is the frequency range between the 3dB cut-off frequencies $f_{c,1}$ and $f_{c,2}$.

$$\zeta = \frac{c}{2\sqrt{mk}} = \frac{\Delta\omega}{2\omega_n} = \frac{\Delta f}{2f_n}. \quad (11)$$

Second, $\zeta \to 0$ seemingly leads to $P_d \to \infty$ and hence infinity power at resonance condition. However, this assumption is invalid as it would lead to excessive relative displacements $z(t)$ and no steady-state conditions. In practice, an energy harvesting system has maximum displacement amplitude Z_{max} of the proof mass as shown in Figure 6. To take this into account, the right-hand side of equation (6) can be rewritten as follows:

$$P_d = \frac{cm^2\omega^4 Y Z_{max}}{2\sqrt{(k-\omega^2 m)^2 + c^2\omega^2}}. \quad (12)$$

Third, regarding equation (6), $P_d \to \infty$ also might be obtained by infinity damping ($\zeta \to \infty$), which is also impossible since the amplitude of the relative motion in equation (4) would be $Z \to 0$ for finite Y. Thus, there would be no relative motion at all. Considering and simplifying the electrical output power from equation (7) at resonance condition, we obtain

$$P_{d,e} = \frac{m\zeta_e Y^2 \omega_n^3}{4(\zeta_e + \zeta_{par})^2}. \quad (13)$$

The relation of the power to the ratio of electrical to parasitic damping ζ_e/ζ_{par} is depicted in Figure 7. The maximum of $P_{d,e}$ is achieved at $\delta P_{d,e}/\delta\zeta_e = 0$, which gives $\zeta_e = \zeta_{par}$.

Since overall damping influences the relative displacement amplitude, ζ has to be adapted to the size of the harvester. The minimum damping should allow an excursion of the proof mass Z near Z_{max} dependent on the target vibrational amplitude Y. With equations (4), (8) and (9) at resonance condition $\omega = \omega_n$, the minimum electric damping ratio for a given generator size Z_{max} can be estimated using

$$Z_{max} = \frac{Y}{2\zeta}. \quad (14)$$

4. POWER CONVERSION IN ELECTROMAGNETIC SYSTEMS

The electromechanical transduction can be realized by applying different conversion approaches. Eligible methods within biomechanical energy harvesting are piezoelectric [19] [20], electrostatic [21], magnetostrictive [22] and electromagnetic conversion techniques.

Electromagnetic generators utilize the production of an electromotive force across an electrical conductor due to a changing magnetic field. The basics for this method are given by Faraday's law of induction. Typically, the conductor takes the form of a coil and the change of the magnetic field is performed by a permanent magnet moving relatively to the conductor. [5] Therefore, the proof mass consists mostly or partly of permanent magnet materials. Since a relative movement is required, either the magnet or the coil can be fixed. However, a moving magnet configuration is more preferred because the coil's wires have to be connected with a fixed load. Since electromagnetic generators have got low output impedance, these systems are characterized by high current and low voltage output levels. [23] Within the field of biomechanical harvesting technologies, most generators apply an electromagnetic transduction mechanism. Examples can be found in Patel et al. [24], Kymissis et al. [25], Zeng et al. [26] and Yie et al. [27]. Though these systems can be flexibly implemented, their bulky sizes and weights inhibit utilization in microelectromechanical systems. Thus, electromagnetic systems are recommended in macro-scale and low-frequency applications. [28]

The modeling and analysis of the electromechanical energy conversion is essential to optimize system parameters and to maximize the power output of the harvester. The following modeling complies with the illustration of a generic electromagnetic energy harvesting system

as depicted in Figure 8. In this configuration, the magnet represents the movable part with mass m.
The governing equation for the electromagnetic system is derived from the general law of motion in equation (2). In addition to the external vibration force $F_a(t) = -m\ddot{y}(t)$, the electromotive force F_{em} opposes the relative motion of the proof mass due to Lenz's law. This force can be described as a function

$$F_{em} = \kappa \cdot I(t) \tag{15}$$

of the induced current $I(t)$ within the coil due to the electromechanical coupling with the coupling coefficient κ. [29] Thus, the obtained differential equation for the mechanical domain becomes

$$m\ddot{z}(t) + c_m\dot{z}(t) + kz(t) = -m\ddot{y}(t) - \kappa \cdot I(t)\ . \tag{16}$$

The damping coefficient c_m defines the damping strictly due to mechanical effects. The governing equation for the electrical domain is given by Kirchhoff's mesh rule in the load circuit consisting of the electrical parameters of the coil (parasitic resistance R_C and inductance L_C) and the applied load R_L:

$$-\kappa\dot{z}(t) + L_C\dot{I}(t) + R_C I(t) + v(t) = 0\ . \tag{17}$$

Therefore, $v(t)$ represents the generated voltage drop at the load due to current $I(t)$:

$$v(t) = R_L \cdot I(t)\ . \tag{18}$$

The induced voltage in equation (17) is proportional to the relative velocity of the magnet and drives current $I(t)$ within the electric domain:

$$V_{ind}(t) = -\kappa \cdot \dot{z}(t)\ . \tag{19}$$

Furthermore, the induced voltage in one coil winding

$$V_{ind,i}(t) = -\frac{d\Phi_i}{dt} \tag{20}$$

is proportional to the rate of change of the flux linkage Φ_i passing through an effective area enclosed by the ith coil winding.

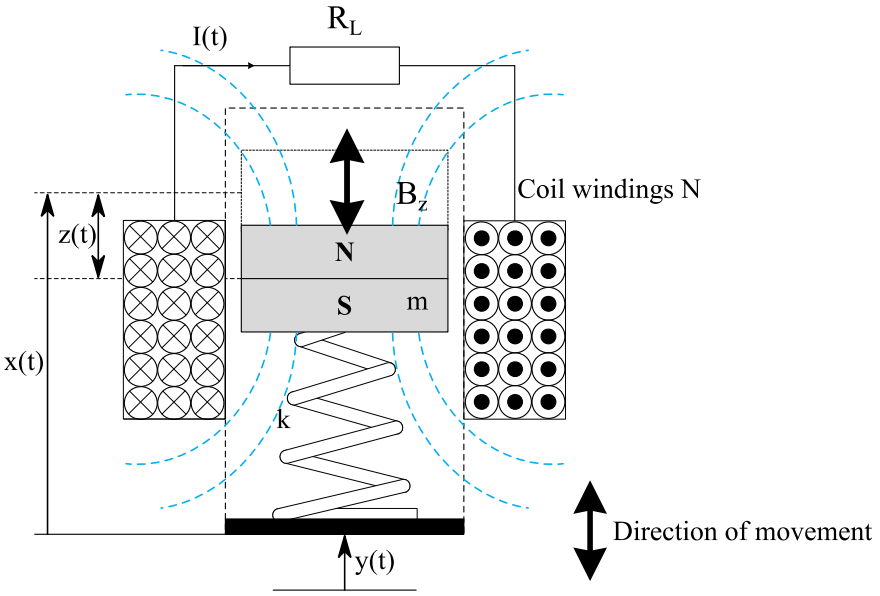

Figure 8: Structure of a single-axis linear electromagnetic energy harvesting system.

In a coil consisting of multiple turns, the total flux linkage

$$\Phi_{\mathrm{tot}} = \sum_{i=1}^{N} \Phi_i \tag{21}$$

is the sum of the linkages for the individual turns. The flux linkage Φ_i of one coil winding can be evaluated by solving the integral of the magnetic flux density B over the area A_i of the ith coil winding. Thus, the total flux linkage results in

$$\Phi_{\mathrm{tot}} = \sum_{i=1}^{N} \int_{A_i} \vec{B} d\vec{A} = N \cdot B \cdot A \cdot \sin\alpha \tag{22}$$

with the angle α between coil area $\vec{A}_i$ and flux density direction $\vec{B}$. We assume that $\vec{B}$ and $\overrightarrow{A_i}$ are arranged orthogonally to each other as shown in Figure 8. Further, the magnetic flux density is uniform over the area of each turn to obtain the simplified form on the right-hand side of equation (22). [30] The total induced voltage becomes

$$V_{ind}(t) = -N \cdot A \cdot \frac{dB}{dt} = -\kappa \frac{dz}{dt}\,, \tag{23}$$

which is equal to equation (19). As a result, the electromechanical coupling coefficient can be expressed as

$$\kappa = N \cdot A \cdot \frac{\mathrm{dB}}{dz} \tag{24}$$

and the induced voltage as

$$V_{ind}(t) = -N \cdot A \cdot \frac{dB}{dz}\frac{dz}{dt}\,. \tag{25}$$

The damping force resulting of electromechanical conversion

$$F_{em} = c_e \cdot \frac{dz}{dt}\,, \tag{26}$$

which opposes the movement of the magnet, is proportional to the current within the electric domain and hence to the velocity. The proportional factor is the electrical damping coefficient c_e. The generated instantaneous power $P_{d,e}$ within the electrical domain can be expressed by using

$$P_{d,e} = F_{em} \cdot \frac{dz}{dt} = c_e \cdot \left(\frac{dz}{dt}\right)^2. \tag{27}$$

In the electrical circuit, this power can be calculated by using the induced voltage V_{ind} and the total electrical impedance of coil and load

$$P_{d,e} = \frac{(V_{ind}(t))^2}{R_L + R_C + j\omega L_C} = \frac{\kappa^2}{R_L + R_C + j\omega L_C} \cdot \left(\frac{dz}{dt}\right)^2. \tag{28}$$

In most cases and especially for low-frequency energy harvesting systems, the term $j\omega L_C$ is neglected since $\omega L_C \ll R_C + R_L$. Furthermore, we assume that equations (27) and (28) are equal and obtain an expression for the damping coefficient as a function of the electromechanical coupling coefficient as well as electrical and magnetic parameters:

$$c_e = \frac{\kappa^2}{R_L + R_C} = \frac{\left(N \cdot A \cdot {}^{dB}/_{dz}\right)^2}{R_L + R_C}. \tag{29}$$

By substituting equations (26) into the governing differential equation (16), we obtain

$$m\ddot{z}(t) + c_m\dot{z}(t) + kz(t) = -m\ddot{y}(t) - c_e \cdot \dot{z}(t) \tag{30}$$

and further with equation (29)

$$m\ddot{z}(t) + c_m\dot{z}(t) + kz(t) = -m\ddot{y}(t) - \frac{\kappa^2}{R_L + R_C} \cdot \dot{z}(t)\,. \tag{31}$$

Thus, high electromechanical coupling coefficients generate a much higher electrical damping within the energy harvesting system. Additionally, low output impedances intensify this effect. Generally, biomechanical generators are macro-scaled systems with relatively heavy proof masses oscillating at low frequencies. Therefore, the electrical damping in equation (31) is much higher than the mechanical damping, which might be neglected so that the load only has to be adjusted to the parasitic impedance of the coil.

5. ELECTROMAGNETIC PARAMETER STUDY

As shown in section 4, the analysis of the electromechanical coupling coefficient κ within energy harvesting systems is crucial to increase the power output since it affects the matching of damping and resistances. According to equation (24), κ is dependent on the change of the magnetic flux density dB/dz along the displacement axis as well as on the design parameters of the coil and magnet. Therefore, we applied a numerical finite element modelling by using the simulation software COMSOL Multiphysics to examine the influence of selected parameters on the output voltage. In our study, an open-circuit analysis was performed, i.e. the current through the coil and load is zero and hence only the induced voltage is considered. The setting of the simulation of the generic electromagnetic generator is depicted in Figure 9. Here, a cylindrically shaped magnet with radius r_M and height h_M is applied inside a coil with N windings. The magnet performs a relative vertical movement within the coil whereby an open-circuit voltage is induced. In this simulation, the root-mean-square voltage

$$V_{rms} = \sqrt{\frac{1}{T}\int_0^T |V_{ind}(t)|^2 dt} \tag{32}$$

is calculated on the basis of a simulated magnetic field (see equations (20) and (21)). Within the parametric study, parameters of the relative movement, coil and the magnet are varied and examined. Standard values of constant parameters are defined in Table 1.

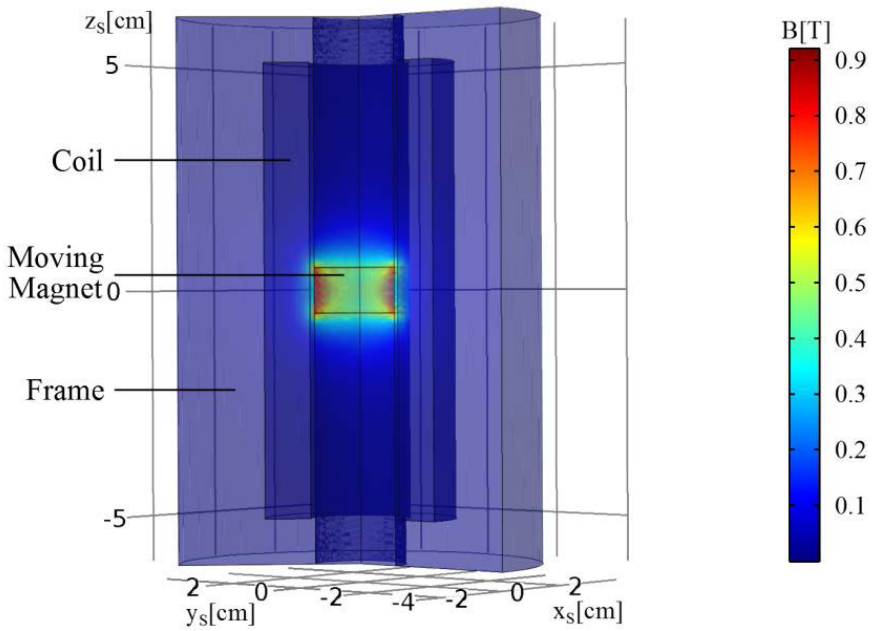

Figure 9: Three-dimensional simulation setting of the generic electromagnetic energy harvesting system with numerical calculation of the magnetic flux density B in Tesla.

Table 1: Variables and standard values.

Parameter	Denomination	Standard value
r_M	Radius of the magnet	10 mm
h_M	Height of the magnet	10 mm
B_r	Remanence of the magnet	1.2 T
r_g	Gap between magnet and coil $(r_C - r_M)$[2]	1 mm
r_C	Radius of the coil[3]	11 mm
N	Coil windings	1000
σ_C	Specific conductivity of the coil	$5.8 \cdot 10^7 \mathrm{S/m}$
A_w	Cross-section area of coil wires	$0.283\ \mathrm{m}^2$
f	Frequency of the magnet movement	1 Hz
Z	Amplitude of the magnet movement	25 mm
Z_{max}	Maximum displacement amplitude	50 mm

5.1 Parameters of relative movement

Within the simulation, the magnet's relative movement is predefined as a harmonic oscillation with $z(t) = Z \cdot (2\pi f t)$. Thus, neither external vibration source nor mechanical power conversion is considered.

Figure 10 shows the variation of induced voltage with respect to the amplitude Z (left) and the frequency f (right) of the relative movement of the magnet. It can be seen that higher displacement amplitudes substantially increases the output voltage. In this case, the generator has a maximal displacement of $Z_{max} = 50$ mm. High induced voltages can be obtained by utilizing the entire length of the generator. Furthermore, the V_{rms} proportionally grows with higher frequency f of the relative displacement due to a rapidly changing magnetic field (see equation (20)). As reminder, the magnet oscillates with the same frequency as the angular frequency ω of the excitation $y(t)$. However, it is more important to match the resonant frequency ω_n to ω since higher relative displacement amplitudes Z (see equation (4)) and hence higher induced voltages (see Figure 10 (left)) can be achieved.

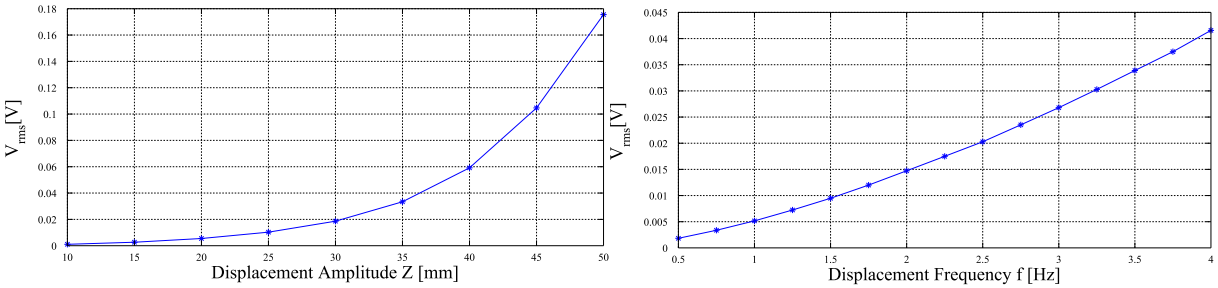

Figure 10: V_{rms} vs. Displacement Amplitude Z (left); V_{rms} vs. Displacement Frequency (right).

5.2 Parameters of the Coil

The simulation of coil parameters is limited to the number of coil windings N due to the consideration of the open-circuit voltage. The coil resistance R_C and the inductance L_C do not affect the output voltage when the current is set to zero, because there is no voltage drop at the coil's internal impedance.

According to equation (25), there is a linear proportional relation between the induced voltage V_{rms} and the number of coil windings N, which is verified by the numerical simulation as depicted in Figure 11. Thus, a higher output voltage is obtained by increasing the number of coil windings. However, more coil windings also increase the internal resistance of the coil since R_C is defined as

[2] A gap of $r_G = 1$ mm is assumed to ensure a movement of the magnet and the installation of a coil body.
[3] The radius of the coil changes with the radius of the magnet while the gap r_G remains constant.

$$R_C = \frac{1}{\sigma_C} \cdot \frac{l_C}{A_w} \tag{33}$$

with the total length of the coil wire $l_C = N \cdot 2\pi r_C$. The parasitic coil resistance can be decreased by using coil wires with higher cross-section areas A_w resulting in a bulkier volume and larger mass.

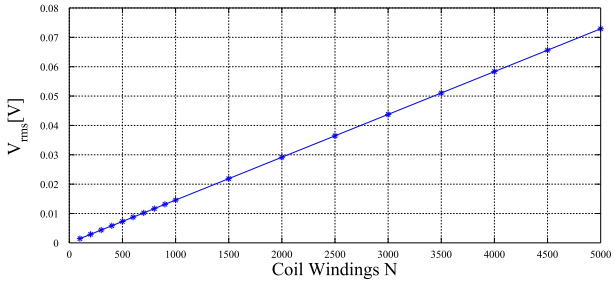

Figure 11: V_{rms} vs. number of coil windings.

5.3 Parameters of the Magnet

Design parameters of the magnet notably influence the produced magnetic field and hence the induced voltage within the coil. Therefore, the radius r_M and height h_M of the magnet as well as the remanence is successively varied.

The variation of the magnet's dimensions has a significant impact on the output voltage, which can be seen in Figure 12 (top). Thereby, increasing the height allows higher output voltages than increasing the radius since more coil windings are exposed to the magnetic field. However, larger heights of the magnet go with smaller displacement amplitudes. The analytic models in section 3 and 4 assume a point mass and do not consider the dimensions of the magnet. Setting the point mass to the center of the magnet, the displacement amplitude is limited by $Z = Z_{max} - h_M/2$. In Figure 12 (bottom right), the induced voltage is shown at maximal displacement amplitude and a variation of h_M. This illustration exhibits a maximum voltage at $h_M \approx 30$ mm, which is approximately one third of the complete length of the generator $2 \cdot Z_{max} = 100$ mm.

Thus, a solution of this optimization problem has to be found. A larger radius r_M additionally entails a larger coil radius r_C and coil area A in equations (22) – (25), which increases the induced voltage and coupling coefficient. As reminder, larger magnet sizes result in enlarged generator dimensions and masses, which easily can affect the human movement. Assuming a constant density of the magnet, the proof mass in equations (7) and (13) rises with larger magnet dimensions, which additionally results in a higher output power within the electromechanical conversion[4].

The remanence or residual magnetism determines the magnetization of magnetic material after removal of an external magnetic field. Typical values for neodymium magnets are $1.0 - 1.47$ T depending on the grade of the magnets (N30 – N52). In contrast, ferrite magnets' remanence only amounts to 0.4 T. Thus, they are not suitable for gaining a high output power in energy harvesting devices. However, the combination of neodymium-iron-boron is currently one of the strongest commercially available magnet materials, which fulfills the requirements of high magnetic fields to generate high induced voltages. In our simulation, the magnetization direction corresponds with the direction of the relative movement (z-direction) as depicted in Figure 8. The change of the remanence of the magnet has a slight proportional effect on the output voltage, which can be seen in Figure 12 (bottom left).

[4] This, however, only applies if the resonant frequency is matched as well.

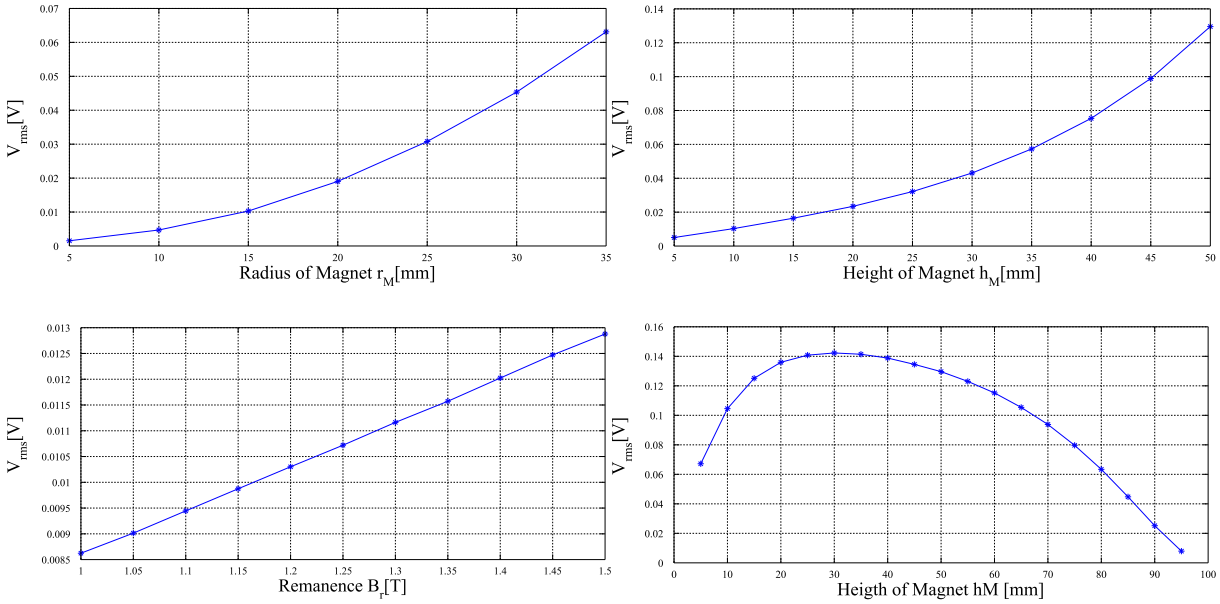

Figure 12: V_{rms} vs. radius of the magnet (top left); V_{rms} vs. remanence of the magnet (bottom left); V_{rms} vs. height of the magnet at fixed displacement amplitude $Z = 25\ mm$ (top right) and at maximal displacement amplitude $Z = Z_{max} - h_M/2$ (bottom right).

6. REQUIREMENTS, CHALLENGES AND DESIGN CRITERIA

After regarding the energy source of biomechanical generators as well as the electromechanical power conversion and electromagnetic parameters, requirements and design criteria can be derived to maximize the power output for appropriate applications. Therefore, the general design, biomechanical characteristics and electromechanical issues are considered.

6.1 General Design Considerations

The groundwork for the adjustment of the generator design is the definition of characteristics of the load as voltage, current and the required power dissipation while, at the same time, minimizing the generator volume and mass to reduce the user's effort. [31] Therefore, a distinction is made between *Harvest-Use* and *Harvest-Store-Use* architectures of energy harvesting systems. In *Harvest-Use* architectures, the generated power directly supplies the electric consumer, which requires a continuous and adjusted power flow from a sufficient energy source. Architectures with one or more storage elements (e.g. capacitors, accumulators) are more common since they ensure a power flow in case of abrupt outages of the energy source. Due to significant variations in human motions, human kinetic energy harvesting systems are based almost exclusively on *Harvest-Store-Use* architectures. This results in complex load impedances, which are characterized by capacitive elements. [32] Additionally, DC power is required to charge appropriate elements. Thus, a rectification of the induced AC voltage of electromagnetic generators has to be performed, which causes additional losses. The low output voltage caused by low load impedances within electromagnetic systems is often insufficient for rectifier diodes, so that transformers have to be applied. Else, high induced voltages have to be achieved by adjusting parameters in equation (25). Both solutions lead to bulkier and more complex generator designs since high induced voltages are obtained by applying more coil windings (see Figure 11) as well as larger coils and magnets (see Figure 12). This in turn limits the mobility of the system's user.

6.2 Biomechanical and Mechanical Design Issues

In general, the design of the mechanical system within biomechanical generators in Figure 6 has to be adjusted to the human movement presented in section 2.2.

First, proper positioning of biomechanical generators at the human body is essential for the determination of the effective driving force of the generator. The highest acceleration magnitudes can be obtained at the ankle during walking and at the ankle and knee during running (see Figure 3). It is obvious that the magnitudes during running are larger than walking. Generators mounted at the ankle are mostly affected by the heel strike during the gait cycle in vertical direction. Appropriate systems mounted at the knee reveal an almost continuous acceleration in vertical and horizontal direction during running. These effects result in different frequency characteristics as can be observed in Figure 3 and Figure 4.

The major issue in vibration harvesting systems is the matching of the system's resonant frequency to the frequency of the vibration source as shown in Figure 7. The excitation of human kinetic energy harvesting systems provides a relatively large frequency range due to the characteristics of human gait. Additionally, the frequency maxima of examined body positions differ from each other and the location of the principal maxima varies over the gait velocity as shown in Figure 5. The ankle's principal maximum varies from 1 Hz to 1.6 Hz and the second maximum from 2 Hz to 3.2 Hz. Further lower maxima appear at whole-numbered multiples of the fundamental frequency. Thus, limitations of the frequency range due to the bandwidth of the generator's mechanical domain causes considerable losses.

According to equation (8), the resonant frequency of the human kinetic energy harvesting system can be matched to the fundamental frequency by adjusting the spring rate k to the proof mass m. For low frequencies of 1 – 1.6 Hz and an assumed proof mass of 0.1 kg, the spring rate is approximately 3.9 – 10 N/m. [12] Stiffer springs can be applied by using a larger proof mass, which in turn increases the generator volume and mass. Furthermore, k and m have to be adjusted together with the total damping coefficient c to set the bandwidth of the system. Applying equations (10), (9) and (8), we obtain

$$2\zeta = \frac{c}{\sqrt{mk}} = \frac{\Delta\omega}{\omega_n}. \tag{34}$$

Within human kinetic energy harvesting systems the damping controls the bandwidth in relation to the resonant frequency. Low resonant frequencies and comparatively high bandwidths result in high overall damping ratios ζ, which in turn cause low output power at resonant condition according to Figure 7 (left). It is recommended to implement an active frequency and damping control to adjust ω_n and c. This would also allow an adaptation of the system to the deployment at different body locations and gait velocities. Though resonant conditions can be achieved, the generated output power within biomechanical generators is limited due to the proportionality to ω_n^3 and comparatively low vibration frequencies. This causes a low-frequency relative movement and hence low induced voltages as shown in Figure 10 (right).

The displacement amplitude of the source vibration Y is another aspect which has to take into account since output power is proportional to Y^2. Within human kinetic energy harvesting, the excitation amplitude is comparatively highly dependent on the height and proportion of the user as well as the way of locomotion. The displacement amplitude also varies at different body locations as depicted in Figure 2, whereby the marker at the ankle exhibits the largest vertical displacements ($\approx$ 10 cm). According to the design of biomechanical generators, the maximal displacement amplitude Z_{max} is associated with Y across the damping ratio ζ at resonant condition (see equation (14)). As shown in Figure 10 (left), Z_{max} should be as large as possible within a known generator frame to maximize the power output. Additionally, it has to be ensured that the proof mass' displacement amplitude Z approaches Z_{max} by adjusting the damping ratio.

6.3 Electromagnetic Design Issues

Due to relatively large masses and low excitation frequencies within biomechanical energy harvesting systems, mechanical damping is much lower than the damping caused by the electromechanical conversion. According to equation (29), the electrical damping is defined by the parasitic and load impedance as well as the electromechanical coupling coefficient κ. High induced voltages and hence maximum output power requires a good electromagnetic coupling, which is proportional to coil and magnet parameters as shown in equation (23). As mentioned in section 6.1, this is achieved by applying a high number of coil windings as well as large coil and magnet dimensions, which increase the generator volume and mass. High coupling coefficients lead to high electrical damping coefficients and hence to lower displacement amplitudes of the moving mass. Thus, an optimization problem has to be solved in designing the electromechanical coupling and damping within human kinetic energy harvesting devices. Additionally, the height of the magnet substantially affects the induced voltage due to a higher magnetic flux density as shown in Figure 12 (top). However, large magnets limit the displacement amplitude Z and the induced voltage as shown in Figure 12 (bottom right). An optimum between the displacement amplitude and the magnet's height has to be found by a given generator volume. The optimization of the magnetic field density within the conductor is another major issue. The coil within the generic configuration in Figure 8 is affected by the magnet's stray field. To maximize the field density, suitable magnet arrangements have to be implemented in order to obtain a strong and homogeneous magnetic field. Hence, high output power can be generated.

Further, the electrical damping due to Lenz's law has to be adapted by controlling the load resistance. In doing so, the power adjustment in the electrical domain also has to be considered to allow an oscillation of the proof mass near Z_{max}. Thus, another optimization problem considering the damping has to be solved, especially with applied complex loads due to rectifier diodes and capacitive storage elements.

7. CONCLUSION

Human kinetic energy harvesting is quite different from machine or vibration energy harvesting due to biomechanical characteristics and generator design requirements. [33] In this paper, we examined the potentials and features of the excitation, the human gait, to derive design requirements as well as challenges within electromagnetic biomechanical generators.

First, the frequency response of the human gait exhibits complex combinations of a large amount of harmonic oscillations with high magnitudes at low frequencies. Furthermore, relatively high excitation displacements are measured. The acceleration magnitudes at the ankle during walking and at ankle and knee during running as well as high displacement amplitudes at these body locations indicate potential power sources within human gait.

The mechanical conversion within biomechanical inertial generators requires an adjustment of the systems parameters to the characteristics of the human locomotion. Therefore, a matching of the system's resonant frequency and bandwidth to the frequency response of the human gait has to be performed in order to maximize the output power. According to Elvin et al. [34], active and passive frequency tuning techniques can be implemented to match the resonant frequency and to widen the bandwidth. Therefore, nonlinear mechanical and magnetic configurations showed high potentials in order to improve the power output.

Due to low resonant frequencies and relatively large bandwidths, high damping ratios have to be applied, which in turn limit the output power at resonant conditions. Furthermore, the total damping ratio is complexly affected by mechanical, electromagnetic and electrical parameters like mechanical damping, electromechanical coupling coefficients and load impedances. Though, high induced voltages require high electromechanical coupling coefficients, damping

is increased by high values for κ. Hence, displacement amplitudes are reduced. Additionally, macro-scale generators with large masses and a high number of coil windings limit the user's mobility, which has to be taken into account. Here, the electrical damping can be adjusted by a matching of the load resistance to the electromechanical coupling to adapt the generator dimension to the vibration amplitude.
Regarding the electromagnetic conversion, parameters were studied and simulated in order to increase the magnetic field density. Therefore, the influence of a variation of parameters on the induced voltage within the coil was examined. Here, an optimization problem between the size of the moving mass and the maximum displacement amplitude by a given generator size was considered.
In summary, maximizing the performance of human kinetic energy harvesting systems requires solutions of multiple optimization problems regarding mechanical (e.g. resonant frequency) and electromagnetic (e.g. damping vs. electromechanical coupling) generator elements. Active control and tuning of selected parameters consume extra power within the system, though suitable methods might significantly increase the output power within biomechanical generators.

REFERENCES

[1] R. Vullers, R. van Schaijk, I. Doms, C. Van Hoof and R. Mertens, "Micropower energy harvesting," *Solid-State Electronics,* vol. 53, pp. 684-693, 2009.

[2] V. Leonov, "Energy Harvesting for Self-Powered Wearable Devices," in *Wearable Monitoring Systems*, New York, Springer, 2011, pp. 27-50.

[3] S. Flipsen, "Alternative Power Sources for Portables & Wearables, Part 1: Power Generation & Part 2:," Delft University of Technology, 2005.

[4] B. Flipsen, A. Bremer, A. Jansen and M. Veefkind, "Towards a Selection Method for Designing Alternative Energy Systems in Consumer Products," in *Proceedings of the TMCE*, Lausanne, Switzerland, 2004.

[5] S. Beeby, M. Tudor and N. White, "Energy harvesting vibration sources for microsystems applications," *Measurement Science and Technology,* vol. 17, pp. 175-195, 2006.

[6] S. Roundy, P. Wright and J. Rabaey, Energy Scavenging for Wireless Sensor Networks with Special Focus on Vibrations, New York, USA: Springer Science+Business Media, 2004.

[7] M. Hannan, S. Mutashar, S. Samad and A. Hussain, "Energy harvesting for the implantable biomedical devices: issues and challenges," *BioMedical Engineering OnLine,* vol. 13, no. 79, 2014.

[8] T. Starner and J. Paradiso, "Human-Generated Power for Mobile Electronics," *Low-Power Electronics Design,* pp. 1-35, 2004.

[9] P. Mitcheson, T. Green, E. Yeatman and A. Holmes, "Architectures for Vibration-Driven Micropower Generators," *Journal of Microelectromechanical Systems,* vol. 13, no. 3, pp. 429-440, 2004.

[10] J. Yun, S. Patel, M. Reynolds and G. Abowd, "Design and Performance of an Optimal Inertial Power Harvester for Human-Powered Devices," *IEEE Transactions on Mobile Computing,* vol. 10, no. 5, pp. 669-683, 2011.

[11] T. von Büren, P. Mitcheson, T. Green, E. Yeatman, A. Holmes and G. Tröster, "Optimization of Inertial Micropower Generators for Human Walking Motion," *IEEE Sensors Journal,* vol. 6, no. 1, pp. 28-38, 2006.

[12] O. Kröning and H. Rothe, "Gait Motion Analysis using Optical and Inertial Sensor Fusion to Design Human Kinetic Energy Harvesting Systems," in *Proceeding of the SPIE Optics+Photonics*, San Diego, 2017 (unpublished).

[13] S. Madgwick, „An efficient orientation filter for inertial and inertial/magnetic sensor arrays," Technical Report, University of Bristol, UK, 2010.

[14] P. Mitcheson, E. Yeatman, G. Kondola Rao, T. Green und A. Holmes, „Energy harvesting from human and machine motion for wireless electronic devices," *Proceedings of the IEEE,* Bd. 96, Nr. 9, pp. 1457-1486, 2008.

[15] C. Williams und R. Yates, „Analysis of a micro-electric generator for microsystems," *Solid-State Sensors and Actuators,* Bd. 1, pp. 369-372, 1996.

[16] M. El-hami, P. Glynne-Jones, N. White, S. Beeby, E. James, A. Brown und M. Hill, „Design and fabrication of a new vibration-based electromechanical generator," *Sensors and Actuators A: Physical,* Bd. 92, Nr. 1, pp. 335-342, 2001.

[17] W. Thomson, Theory of Vibration with Applications, Taylor & Francis, 1996.

[18] N. Stephen, „On energy harvesting from ambient vibration," *Journal of Sound and Vibration,* Bd. 293, pp. 409-425, 2006.

[19] M. Renaud, P. Fiorini, R. van Schaijk und C. van Hoof, „Harvesting energy from the motion of human limbs: The design and analysis of an impact-based piezoelectric generator," *Smart Material and Structures,* Bd. 18, Nr. 3, 2009.

[20] G. Bassani, A. Filippeschi und E. Ruffaldi, „Human motion energy harvesting using a piezoelectric MFC patch," in *37th Annual International Conference of the IEEE Engineering in Medicine and Biology Society (EMBC)*, Milan, Italy, 2015.

[21] Y. Naruse, N. Matsubara, K. Mabuchi, M. Izumi und S. Suzuki, „Electrostatic micro power generation from low-frequency vibration such as human motion," *Journal of Micromechanics and Microengineering,* Bd. 19, Nr. 9, 2009.

[22] L. Wang und F. Yuan, „Energy harvesting by magnetostrictive material (MsM) for powering wireless sensors in SHM," in *14th International Symposium of SPIE Smart Structures and Materials & NDE and Health Monitoring*, 2007.

[23] T. Kazmierski und S. Beeby, Energy Harvesting Systems - Principle, Modeling and Applications, New York, USA: Springer, 2011.

[24] P. Patel und M. Khamesee, „Electromagnetic micro energy harvester for human locomotion," *Microsystem Technologies,* Bd. 19, pp. 1357-1363, 2013.

[25] J. Kymissis, C. Kendall, J. Paradiso und N. Gershenfeld, „Parasitic Power Harvesting in Shoes," *Second IEEE International Conference on Wearable Computing,* pp. 132 - 139, 1998.

[26] P. Zeng, H. Chen, Z. Yang und A. Khaligh, „Unconventional Wearable Energy Harvesting from Human Horizontal Foot Motion," in *26th Annual IEEE Applied Power Electronics Conference and Exposition (APEC)*, Fort Worth, TX, 2011.

[27] L. Xie und M. Cai, „Human Motion: Sustainable Power for Wearable Electronics," *IEEE Pervasive Computing,* Bd. 13, Nr. 4, pp. 42 - 49, 2014.

[28] G. Poulin, E. Sarraute und F. Costa, „Generation of electrical energy for portable devices: Comparative study of an electromagnetic and a piezoelectric system," *Sensors and Actuators A: Physical,* Bd. 116, pp. 461 - 471, 2004.

[29] S.-D. Kwon, J. Park und K. Law, „Electromagnetic energy harvester with repulsively stacked multilayer magnets for low frequency vibrations," *Smart Materials and Structures,* Bd. 22, Nr. 5, 2013.

[30] S. Beeby und T. O'Donnell, „Electromagnetic Energy Harvesting," in *Energy Harvesting Technologies*, New York, USA, Springer Science+Business Media, 2009, pp. 129 - 164.

[31] N. Awaja, D. Sood und T. Vinay, „Design and Analyses of Electromagnetic Microgenerator," *Sensors & Transducers Journal,* Bd. 103, Nr. 4, pp. 109 - 121, 2009.

[32] S. Sudevalayam und P. Kulkarni, „Energy Harvesting Sensor Nodes: Survey and Implications," *IEEE Communications Surveys & Tutorials,* Bd. 13, Nr. 3, pp. 443 - 461, 2011.

[33] D. Zhu, „Vibration Energy Harvesting: Machinery Vibration, Human Movement and Flow Induced Vibration," in *Sustainable Energy Harvesting Technologies - Past, Present and Future*, Y. Tan, Hrsg., InTech, 2011.

[34] N. Elvin and A. Erturk, Advances in Energy Harvesting Methods, New York, USA: Springer Science+Business, 2013.

CONTACTS

O. Kröning, M.Sc. oliver.kroening@hsu-hh.de
Prof. Dr.-Ing. habil. H. Rothe rothe@hsu-hh.de